# Analyzing Surfactant Structures on Length and Chirality Resolved (6,5) Single-Wall Carbon Nanotubes by Analytical Ultracentrifugation

**Jeffrey A. Fagan,[†,*] Ming Zheng,[†] Vinayak Rastogi,[†,⊥] Jeffrey R. Simpson,[‡] Constantine Y. Khripin,[†] Carlos A. Silvera Batista,[†] and Angela R. Hight Walker[§]**

[†]National Institute of Standards and Technology, Materials Science and Engineering Division, 100 Bureau Drive, Gaithersburg, Maryland 20899, United States, [‡]Department of Physics, Astronomy and Geosciences, Towson University, Towson, Maryland 21252, United States, and [§]National Institute of Standards and Technology, Semiconductor and Dimensional Metrology Division, 100 Bureau Drive, Gaithersburg, Maryland 20899, United States [⊥]Present address: (V.R.) Tokyo Electron Technology Center America, Albany, NY 12203.

**ABSTRACT**

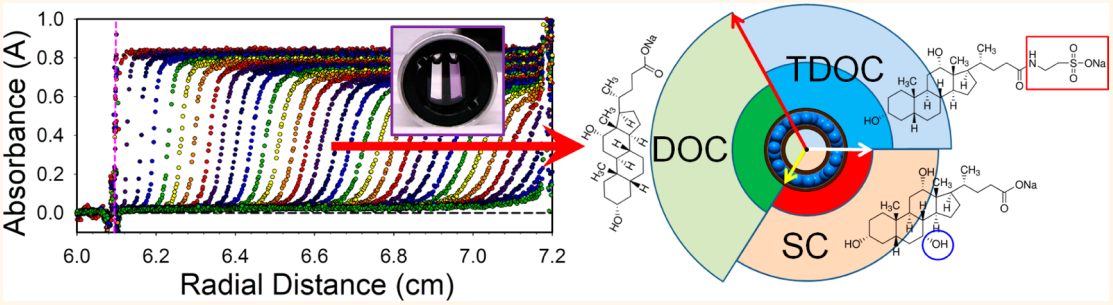


The structure and density of the bound interfacial surfactant layer and associated hydration shell were investigated using analytical ultracentrifugation for length and chirality purified (6,5) single-wall carbon nanotubes (SWCNTs) in three different bile salt surfactant solutions. The differences in the chemical structures of the surfactants significantly affect the size and density of the bound surfactant layers. As probed by exchange of a common parent nanotube population into sodium deoxycholate, sodium cholate, or sodium taurodeoxycholate solutions, the anhydrous density of the nanotubes was least for the sodium taurodeoxycholate surfactant, and the absolute sedimentation velocities greatest for the sodium cholate and sodium taurodeoxycholate surfactants. These results suggest that the thickest interfacial layer is formed by the deoxycholate, and that the taurodeoxycholate packs more densely than either sodium cholate or deoxycholate. These structural differences correlate well to an observed 25% increase in fluorescence intensity relative to the cholate surfactant for deoxycholate and taurodeoxycholate dispersed SWCNTs displaying equivalent absorbance spectra. Separate sedimentation velocity experiments including the density modifying agent iodixanol were used to establish the buoyant density of the (6,5) SWCNT in each of the bile salt surfactants; from the difference in the buoyant and anhydrous densities, the largest hydrated diameter is observed for sodium deoxycholate. Understanding the effects of dispersant choice and the methodology for measurement of the interfacial density and hydrated diameter is critical for rationally advancing separation strategies and applications of nanotubes.

**KEYWORDS:** carbon nanotube · analytical ultracentrifugation · SWCNT · bile salt

Single-wall carbon nanotubes (SWCNTs) in aqueous solutions containing surfactants have been widely investigated over the past decade. While initial studies primarily focused on improving the measured optical and physical properties of directly dispersed SWCNTs through enhanced isolation and stability in dispersion,[1,2] the emphasis of more recent contributions has shifted to enabling the separation of individual nanotube species[3−9] (chiralities) and/or lengths from mixed populations[10−13] to improve the realizable material properties.[14] In particular, separation of different nanotube species based on the variation of their buoyant densities in a density gradient for various surfactant and cosurfactant mixtures has been widely studied.[15−17] However, although

* Address correspondence to jeffrey.fagan@nist.gov.

Received for review January 15, 2013 and accepted March 26, 2013.

**Published online March 26, 2013**
**10.1021/nn4002165**

© 2013 American Chemical Society

a significant number of empirical recipes are available for separating specific nanotubes, the basis for predictive determination of separation strategies does not yet exist. This is particularly true for variation of the dispersant used to disperse the nanotubes, which is often chosen independently to impart control over specific properties such as the location of optical transitions, selectivity for specific SWCNT species or enantiomers, or robustness in processing. Critically, the information that is missing to enable rational design of nanotube processing, and for prediction of their optical properties, is the structure of the bound dispersant layer on the nanotube surface, and the size of its associated hydration shell.

Here, we present the characterization of the external surfactant packing density and hydration shell properties for the (6,5) SWCNT as determined by analytical ultracentrifugation (AUC) in multiple common bile-salt surfactant solutions. The surfactants examined are sodium deoxycholate (DOC), sodium taurodeoxycholate (TDOC), and sodium cholate (SC); chemical structures are shown in Figure 1. The concentration of the surfactant was kept constant in all experiments at 10 g/L. These particular surfactants were chosen based on their common use in SWCNT dispersion and density gradient separations,[6] and their compatibility with our surfactant exchange protocol for transfer without damaging the dispersion quality. The benefit of choosing this set of surfactants is that SC and TDOC are single point chemical mutations from the structure of DOC. Thus, they provide a good model set for future simulations of dispersant packing structures on SWCNTs. Another benefit is that other single point mutation bile salts are purchasable at the gram scale, such that this data set can be expanded with future work; insufficient separated SWCNT sample was available to include the other surfactants in this contribution.

Initial work on noncovalently solubilizing SWCNTs in aqueous dispersion typically used sodium dodecyl sulfate (SDS)[18] or sodium dodecyl benzyl sulfate (SDBS)[19] as the solubilizing surfactant, although many different other dispersants were explored as well. However, most dispersants only fully individualize nanotubes at low SWCNT concentrations, or are prohibitively expensive, and thus are not useful for applications requiring significant concentrations of SWCNTs or greater mass throughput. Wenseleers *et al.*[2] however demonstrated that relatively inexpensive bile salt surfactants were capable of both dispersing individualized SWCNTs and stabilizing them against bundling and reaggregation at increased concentrations. In particular, DOC and TDOC were found to yield superior dispersions at concentrations up to at least 1 mg/mL, and that the SWCNTs in these surfactants displayed improved optical properties as compared to earlier surfactants or several other cholate derivatives. Much of the increase in use of bile salt surfactants though has been driven by their usefulness for density gradient ultracentrifugation (DGU) based separations.

Arnold *et al.*[6] demonstrated the use of bile salt surfactants, particularly SC and SC:SDS mixtures, to achieve scalable diameter, chirality, or metallicity separation through tailored application of DGU. This seminal work has been expanded upon, and many contributions have described refined separation of SWCNT populations by diameter, chirality, enantiomeric handedness,[20] wall number, interior hydration,[21,22] metallic nature, degree of bundling,[23] and length distribution by related methods. Significant disagreements however exist over the mechanisms for some of these separations,[24,25] and refinement has been accomplished by empirical extrapolation and variation of parameters rather than by rational design. The key knowledge gap is in specifying force fields for interactions between individual SWCNT species and a given surfactant, and validating that these give a correct description of the experimentally measured interfacial structure.[26]

Recently Arnold *et al.*[27] explored the use of AUC to determine the packing density of sodium cholate on the surface of chirality separated (6,5) nanotubes. In the most prevalent manner of AUC, the time-dependent spatial distribution of a dispersed species or particle is monitored through optical methods during sedimentation in response to an applied acceleration; this is referred to as a sedimentation velocity experiment.[28] The rate of sedimentation of particles in dilute dispersions is primarily affected by the density difference of the particle to the solvent, the particle shape and size, and the solution viscosity. From variation of the aqueous medium density through the use of $D_2O$ exchange, Arnold *et al.*,[27] and later Backes *et al.*,[29] estimated the anhydrous density of the SC-SWCNT complex and used this value to calculate a packing density of the surfactant on the SWCNT surface. Although ground breaking, the limited experimental data (2 points each), the measurement in a single bile salt surfactant, and the width of the sedimentation coefficient distributions in both instances limit the applicability of the information gained.

In this contribution, we perform extensive sedimentation velocity experiments in multiple compositions of $H_2O$, $D_2O$ and $D_2{}^{18}O$ to narrow the measured value for the anhydrous density[30] of the (6,5) SWCNT−surfactant complex in multiple related bile salt surfactants, and utilize a single parent dispersion of both length and chirality sorted SWCNTs that dramatically increases the resolution of the sedimentation coefficient. Comparisons of the experimental data for the different surfactants provide a basis for addressing the underlying causes of optical property differences for dispersions in the only slightly different solution environments. Furthermore, we extend the technique of AUC for SWCNTs to measure the hydrated buoyant density of the SWCNT−surfactant complex, yielding additional information about the size of the hydrated SWCNT *in situ* in the chemical environment used for DGU separations. Combined, these data allow unprecedented resolution of the surfactant structure on the

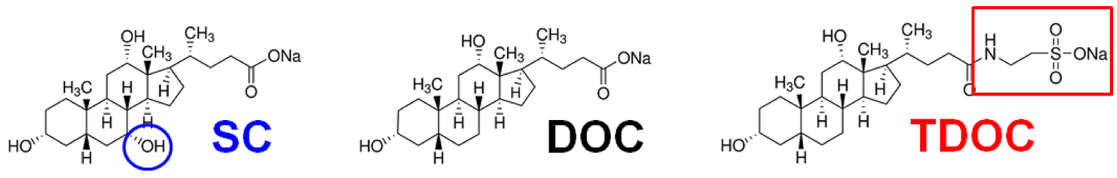


**Figure 1. Surfactant structures for the three bile salt surfactants used in this work. The single points of variance from the structure of DOC for the alternate two surfactants are denoted by the call-outs.**

SWCNT interface, and demonstrate conclusively that AUC will be an important tool for characterizing SWCNT dispersions.

## THEORY

Excluding a dependence on multibody interactions or other external fields in a buoyancy driven separation, the sedimentation rate of a specific nanotube is expected to be a function of four factors, the packing density and structure (size) of the surfactant layer and associated hydration layer surrounding the nanotube, the degree of bundling with other nanotubes, the density of the interior core of the nanotube, and the length of the nanotube. Utilizing the assumption that particles of this size scale rapidly reach terminal velocity for an applied force, the sedimentation can be described by (depending on the preferred definition of the analyte as a solvated molecule, or as a solid particle)[28,30]

$$S = \frac{M(1 - \bar{\nu}\cdot\rho_s)}{N6\pi\eta a f/f_0} = \frac{V_p\cdot(\rho_p - \rho_s)}{6\pi\eta a f/f_0} \quad (1)$$

In eq 1, $M$ is the molar mass, $\bar{\nu}$ is the anhydrous partial specific volume of the molecule, $\eta$ is the viscosity, $a$ is the equivalent hard sphere hydrodynamic radius, $f/f_0$ is the ratio of the friction coefficient divided by the friction coefficient of a hard sphere, and $S$ is the sedimentation coefficient. In the particle definition that we will use, $V_p$ is the volume of the nanotube, $\rho_p$ is the effective density of the SWCNT, and $\rho_s$ is the density of the aqueous medium. $S$ is defined as:

$$S = u/\omega^2 R \quad (2)$$

in which $u$ is the particle velocity, $\omega$ is the rotation rate (in rad/s), and $R$ is the distance from the axis of rotation; the quantity $\omega^2 R$ is thus the applied acceleration.

Using eq 1, and assuming that the structure and hydration of the bound surfactant layer is not altered by the change from $H_2O$ to $D_2O$,[31] variation in the sedimentation coefficient with the change in the medium density can be used to extract the anhydrous (or unsolvated for dispersions in organic solvents) density of the sedimenting particle without explicit knowledge of the particle size. This is done by elimination of common terms in eq 1 for any two compositions of water and $D_2O$, denoted by the subscripts in eq 3.

$$\rho_p = \frac{\eta_1 S_1 \rho_{s,2} - \eta_2 S_2 \rho_{s,1}}{\eta_1 S_1 - \eta_2 S_2} \quad (3)$$

The key feature of this equation is that contributions from the particle size and shape are eliminated for calculation of the anhydrous density. Note: this is the anhydrous density of the particle if the medium parameters are varied only through the composition variation between $H_2O$ to $D_2O$ and the hydration of the particle does not change; more generally, the equation yields the inverse apparent partial specific volume, which is an operationally defined quantity.[30] An important point about eq 3 is that the densities and viscosities of each solution must be known accurately to apply the equation.

There are also several other issues that impact the application of eq 3. Specifically, the experimentally accessible density variation we can achieve for water is limited. For SWCNT-bile salt complexes, the maximum achievable density of the surfactant solution (by using $D_2{}^{18}O$) is substantially less than the anhydrous density of the SWCNT complex; thus, the calculated anhydrous density is highly susceptible to small uncertainties in the values of the medium properties and the measured sedimentation coefficients. Second, the $S$ values identified at both densities must be representative of the same fractional population of the particles for eq 3 to be valid. For example, a mixture of particles with a distribution of anhydrous densities and sizes could have very different sedimentation coefficient distribution shapes for solution densities very different from, or close in value to, one or more of the components. This would lead to uncertainty over the choice of the $S$ value that represents the common mode of the distribution in each solution. Separately, confusion can occur in defining a peak value for a sample with wide and/or flat distributions of sedimentation coefficients. Fortunately, these last two problems are less likely to occur for dispersions of rod-like particles with constant diameters, such as SWCNTs, and particularly for length and chirality separated populations such as ours in which the density of the particles is likely similar and invariant with the particle size (*i.e.*, length).

An equivalent method to eq 3 for extracting the anhydrous density, and one that allows addressing or remediation of the issues noted above, is to fit a line to a set of viscosity corrected sedimentation coefficients measured at multiple compositions of $H_2O$ and $D_2O$ ($D_2{}^{18}O$). The anhydrous density of the complex is then the density at which the fit line extrapolates to $S\eta = 0$; *i.e.*, the density of the medium at which the particle is

neutrally buoyant and neither sediments nor creams. Beyond making use of additional points to better specify the intercept, this method yields additional benefits for analysis. This is the methodology we will use to determine both the anhydrous density and the hydrated buoyant density of the surfactant SWCNT complexes.

## RESULTS AND DISCUSSION

**Characterization of the Sample.** From the theoretical description of sedimentation, it is clear that, although not necessary, a narrower sedimentation coefficient distribution is preferred to enable the extraction of parameters for specific particles rather than distribution averaged values. Thus, for these experiments, we performed a succession of particle processing steps, including rate-zonal ultracentrifugation steps (see Methods), to isolate a length and chirality separated population of SWCNTs. A photograph of the isolated, primarily (6,5) species, long SWCNT dispersion is shown in Figure 2. As has been frequently noted for well-dispersed and purified SWCNT populations, the color of the dispersion is not black but is instead strongly colored, reflective of the specific wavelengths absorbed by the intrinsic optical transitions of the nanotubes.

To demonstrate the degree of chirality separation, and to choose the appropriate wavelength for concentration observation in the AUC, we performed spectroscopic characterization of the sample by absorbance, fluorescence, and Raman spectroscopies. UV−visible-near-infrared (UV−vis-NIR) absorbance spectra of the isolated length and chirality sorted (6,5) nanotubes in DOC is shown in Figure 3A. The spectra of the SWCNTs dispersed in TDOC and SC are shown in the Supporting Information and are essentially indistinguishable, baring slight peak shifts and scaling for concentration, from the DOC dispersed spectra. Immediately apparent in Figure 3A is the size of the absorbance peak features due to the (6,5) SWCNT relative to the underlying background ($A$ (981 nm)/$A$ (775 nm) ≅ 18.5), and the relative paucity of optical transitions due to other SWCNT species. Although NIR fluorescence measurements (Figure 3B, Supporting Information Figures S3 and S4) and the presence of small features in the absorbance spectra indicate that other SWCNT species are present, we estimate that the (6,5) SWCNT is approximately 80−85% of the population based on the fractional contribution of the (6,5) to the total peak absorbance in the visible region of the spectra. From the absorbance and fluorescence spectra, we estimate that the most prevalent contaminant chiralities include the (8,3), (9,1), and (7,5).[32] The positions of the optical transitions also indicate that the SWCNTs are water-filled,[33] which is consistent with our expectations for this SWCNT source, and the observation that the larger diameter SWCNTs displayed greater buoyant densities during the chirality separation.[21] Further optical characterization by resonant Raman spectroscopy is shown in Figure 3C.

**Figure 2. Photographs of the separated, (6,5) rich, length sorted SWCNT population used in this work (1 mm path length), and as diluted for measurement in the sector-shaped AUC cell. The dispersion is richly colored due to the strong intrinsic optical transitions of the SWCNTs, and the high purity of the sample.**

In addition to the (6,5) radial breathing mode (RBM) at 310 $cm^{-1}$,[33,34] the high quality of the sample is indicated by the small D/$G^+$ ratio, which is ≅ 0.014 (peak/peak).

To characterize the length distribution of the length-sorted SWCNTs, atomic force microscopy (AFM) was performed. The number-average mean length and the standard deviation of the mean for the >200 measured nanotubes was 1190 ± 34 nm, with the median number-average length ≅ 950 nm. Values for the mass-average mean and median lengths are greater, with the mean ≅ 1400 nm and the median length ≅ 1050 nm. The width of the distribution was estimated by the calculated standard deviation of the number-average mean length, which was 496 nm. Although this distribution is not perfectly monomodal, the effects of length on the sedimentation coefficient decrease at increased aspect ratios for rods. Explicitly, the sedimentation coefficient scales approximately with $\ln(L/r_{hydro})$, in which $L$ is the rod length and $r_{hydro}$ is the effective hydrodynamic radius of the rod.[35] Assuming this scaling and $r_{hydro}$ < 5 nm, the length distribution observed by AFM should impart a width to the sedimentation coefficient distribution of only approximately 15% of the measured mean $S$ value. Representative AFM images and a histogram of the observed lengths are reported in the Supporting Information.

**Analytical Ultracentrifugation Characterization.** AUC is a powerful technique for the characterization of dispersed polymers, biomolecules, and nanoparticles.[36−41] In the sedimentation velocity experiments performed for this work, an initially homogeneous volume of the SWCNT−surfactant sample was centrifuged at high speed, resulting in the sedimentation of the SWCNTs as a function of time. In an AUC, the spatially varying concentration is recorded using optical methods, either absorbance, fluorescence or through interference optics depending on the sample and the instrumental capabilities. For our experiments, we utilized the absorbance detector, as the sensitivity to the SWCNT concentration was much greater than for the interference optics. Additionally,

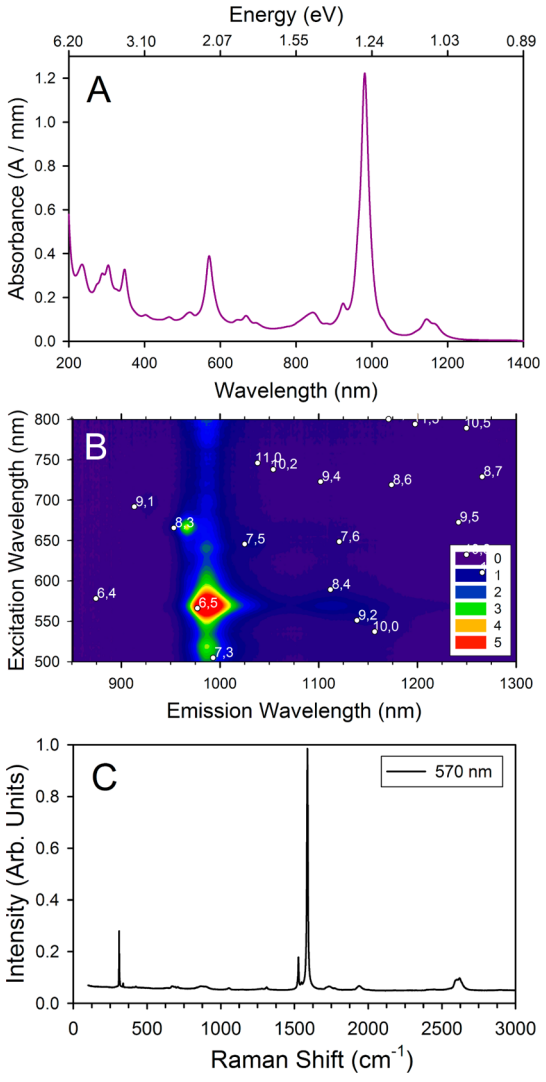


**Figure 3. (A) Absorbance spectrum of the isolated (6,5) SWCNT dispersion used for this work in DOC. The optical transitions are dramatically enhanced by the separation processes due to the removal of impurities, bundled and damaged SWCNTs, and the chirality separation. (B) Excitation−emission contour plot of the NIR fluorescence of the isolated population in DOC surfactant. The (6,5) is the dominant observed species, but small contributions from the (8,3) as well as the (9,1), (7,5), and (9,2) are observed at low concentration. The intensity scale is set equal to 10 at the peak (6,5) $E_{22}$ excitation. Labeled points are assignments from ref 32. (C) Resonant Raman scattering at 570 nm excitation. The $G^+$, $G^-$, and RBM features are clearly visible; the prominent RBM feature at ≅310 $cm^{-1}$ is due to the (6,5) species. The spectrum is offset 0.05 from the axis for clarity. The D/$G^+$ ratio (peak/peak) is ≅ 0.014.**

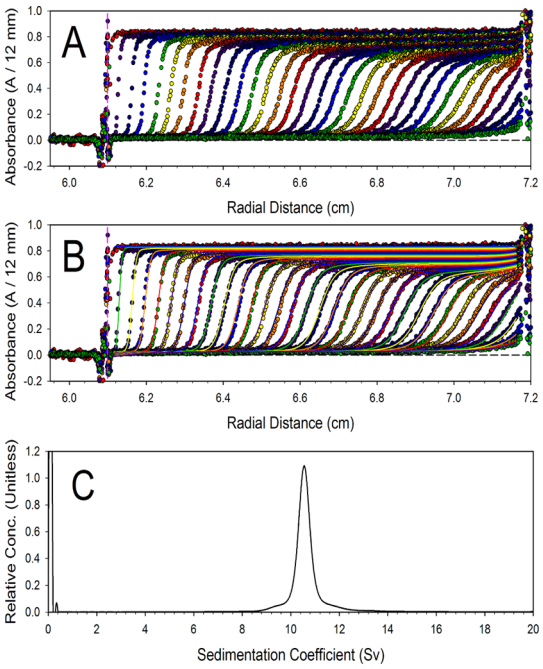


**Figure 4. (A) Radial absorbance scans ($\lambda$ = 235 nm) during centrifugation of the (6,5) SWCNTs in $H_2O$−DOC at 2932 rad/s; shown at 10 min intervals. The (6,5) sediments at these conditions, which causes the concentration boundary to move to larger radial positions with time. Broadening of the boundary is due to a combination of diffusion and the width of the length distribution. The solution meniscus is demarcated by the vertical pink line. (B) The data of panel A showing the best fit lines as solved for using SEDFIT (using all data). The fit lines accurately represent the data. (C) The regularized distribution of sedimentation coefficients (0.683) that produces the absorbance profiles fits shown in panel B.**

the absorbance optics permit selection of the wavelength to be monitored; this allowed for measurements to be made on dispersions containing iodixanol, which generates large (on the instrumental scale) refractive index gradients, but negligibly absorbs light at wavelengths longer than 400 nm. In the absence of iodixanol,[42] no differences in the extracted sedimentation coefficient distribution were observed based on the wavelength chosen for the absorbance monitoring (235, 305, 347, or 570 nm corresponding to the $\pi$, $E_{44}$, $E_{33}$, or $E_{22}$ optical transitions). Most measurements were conducted at 235 ± 2 or 305 ± 2 nm, except in the case for solutions containing iodixanol, which were measured at 570 nm, as instrumental factors lead to lower noise levels when using shorter wavelengths. Unless otherwise noted, uncertainty in this contribution is represented by error bars equal to one standard deviation of the reported value.

A representative series of absorbance profiles, measured at 10 min intervals, for the SWCNT sample dispersed in 10 g/L DOC in $H_2O$ are shown in Figure 4A. As time progresses, the boundary between the SWCNT containing and depleted zones shifts to greater radial distances and broadens, reflecting the distribution of sedimentation coefficients in the sample, and to a lesser extent diffusion. The upper absorbance plateau decreases with time due to radial dilution (*i.e.*, the volume of a sector shaped cell increases with radius).

From the measured concentration profiles, such as those shown in Figure 4A, the distribution of sedimentation coefficients was determined using the analysis package SEDFIT.[43,44] As a basic overview, SEDFIT solves the Lamm equation, eq 4, for the concentration distribution for each elapsed time in the absence of bulk convection within the discretized input range of sedimentation values. The software identifies which *S* values

are observed in the data, the relative weight of those values, and provides regularization to report the distribution of coefficients that equivalently generate the same concentration profile. For those interested, a substantial number of publications report the details of the software package and its advanced capabilities.[45] Details of the fitting as applied for this contribution are reported in the Methods section.

$$\frac{\partial c}{\partial t} = D\left(\frac{\partial^2 c}{\partial R^2} + \frac{1}{R}\frac{\partial c}{\partial R}\right) - \omega^2 S\left(R\frac{\partial c}{\partial R} + 2c\right) \quad (4)$$

In eq 4, $R$ is the distance from the center of rotation, $\omega$ is the rotational frequency, $D$ is the diffusion coefficient, $C$ is the concentration, and $S$ is the sedimentation coefficient. Fit lines to the data set shown in Figure 4A (including profiles not shown) as calculated by SEDFIT are reported in Figure 4B, and the distribution of sedimentation coefficients that generate the fit lines are shown in Figure 4C.

The distribution of sedimentation coefficients in Figure 4C is substantially narrower (full width at half max ≡ fwhm ≈ 1 Sv) than in the two previous reports for SWCNTs with AUC (fwhm ≅ 4 Sv,[27] fwhm ≅ 6 Sv[29]) due to the separation for both length and chirality in this sample (both literature results are for SC). Moreover, in the separation processes used to generate our sample, the SWCNTs were forced to move both toward a lower density zone (length separation), and higher density zone (chirality separation) by the designs of the separations. This encourages removal of impurities, including morphological impurities such as bundles that tend to exhibit greater densities,[23,46,47] and are therefore particularly selected against in the length separation.

In Figure 5, the sedimentation coefficient distributions of the SWCNT sample in DOC are presented for five experiments with increasing $D_2O$ content of the solvent. As expected for a sample with a constant population and morphology, the shape of the distribution remains similar in all of the solvent compositions; the narrowing of the distribution on the absolute scale of the figure is due to the slower velocity of the SWCNTs in compositions with greater $D_2O$ content. Measuring a consistent moment of these sedimentation coefficient distribution as a function of the applied solution parameters allows determination of the anhydrous density of the SWCNTs. The narrowness of the distributions allows for the specification of these moments, such as the most likely sedimentation coefficient, to be monitored at high resolution.

*Anhydrous Density Determination.* For proper comparison of the sedimentation rate to the density change, it is important that a consistent moment of particle distribution is monitored. Multiple methodologies were used to calculate equivalent moments of each distribution, such as those shown in Figure 5, in

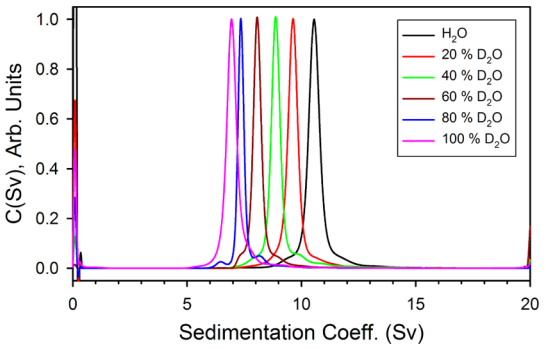


**Figure 5. Sedimentation coefficient distributions for the (6,5) SWCNT sample in DOC as measured for different amounts of $D_2O$ in the medium. As the density difference between the SWCNTs and the solvent decreases with the isotope exchange (and the viscosity increases), the $S$ distribution shifts to smaller absolute values, *i.e.*, sedimentation is slowed.**

the range of 2−18 Sv, including using the peak measured value, a Gaussian fit to the distribution, and the average value of the sedimentation coefficient—thresholding the averaged values at either 10% or 20% of the peak value (to exclude portions of the distribution more prone to signal-to-noise error and fitting variation). Although slightly different values of the mean sedimentation coefficient are measured by each of the various methods (typically within 0.1 Sv of each other), the method used was not found to significantly affect the extrapolated anhydrous density. The extracted values by the four methodologies are shown in Figure 6A. Portions of the sampled sedimentation coefficient range were excluded on the basis that contributions below 2 Sv are primarily sampling artifacts due to the fact that the applied centrifugation rate and time are insufficient to adequately report on the concentration of objects with these $S$ values. Contributions above 18 Sv, small in all measurements, are likely due to a small number of aggregates (which may have a distinct anhydrous density), and thus were inappropriate to include in the calculation. The peak sedimentation values for the SWCNT sample in each surfactant−$D_2O$ fraction composition, as determined by the Gaussian fitting method and multiplied by the solution viscosity, are presented in Figure 6B.

Presenting the $S \cdot \eta$ *versus* solution density data as in the Figure 6 panels causes the value for the anhydrous density to be obvious, see eq 1, but also provides additional information. The high degree of linearity in the data supports the hypothesis that neither preferential hydration in the interior cavity (of $H_2O$ or $D_2O$) nor changes to the surfactant shell structure occur with the transition from $H_2O$ to $D_2O$. That the data points in $D_2{}^{18}O$ mixtures for DOC (two highest density points) continue to fall on the same linear trendline further indicates that H−D exchange is not important; this effect would saturate at 100% D, and a break in the density trendline would be expected with the

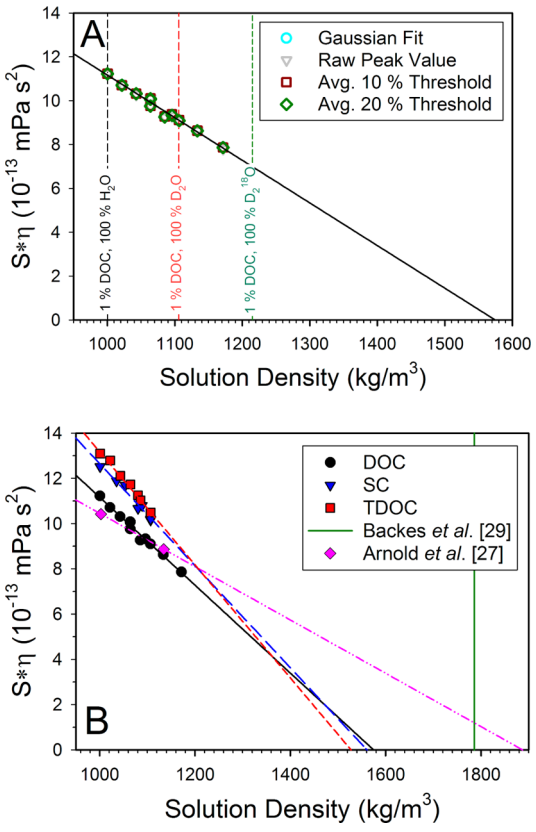


**Figure 6. Viscosity-corrected mean sedimentation coefficients for the (6,5) SWCNTs *versus* the density of the medium as adjusted by the amount of $D_2O$ or $D_2{}^{18}O$ in the solvent at a constant surfactant concentration of 10 g/L. Error bars in both axes are smaller than the symbols. (A) Comparison of the *S* values extracted by the different methodologies from the sedimentation coefficient distribution. The methodology does not significantly affect the extracted value for this sample. (B) For each of the three surfactants, DOC (black points, solid fit line), SC (blue points, long dashes), and TDOC (red points, short dashes), the data is well fit by a straight line, indicating the surfactant structure is not being altered by the change from $H_2O$ to $D_2O$. From the slope of the change in $S\cdot\eta$ with the solution density, the anhydrous density of the SWCNT−surfactant complex can be extracted; the anhydrous density is the density at which $S\cdot\eta = 0$. For comparison, values from Arnold *et al.*[27] (pink diamonds, dash-double dots) and Backes *et al.*[29] (solid vertical line) for the anhydrous density of chirality but not length sorted (6,5) in SC and for an unsorted, but (6,5) biased SWCNT sample, in SC, respectively, are shown.**

transition to $D_2{}^{18}O$. Propagating the uncertainty in the density and viscosities, and assuming a linear fit with independent errors, the values of the anhydrous density for the SWCNT sample in 10 g/L surfactant are given in Table 1. Effective uncertainty in the sedimentation coefficient values for uncertainty propagation was calculated from the DOC data points assuming the linear fit was exact; this value, ± 0.12 Sv, was larger than the error calculated by methods on individual points within SEDFIT (although still smaller than the symbols in Figure 6). Comparing the quality of the experimental data we gather for SWCNTs to that reported for the most common application of AUC, *i.e.*, biological molecules, the sharpness of our sedimentation coefficient distributions is reasonably equivalent to that of a protein such as phosphorylase B.[43] However, the uncertainty we will calculate for the anhydrous density will always be intrinsically larger (given the same number of data points, *etc.*) for our experiments because the intercept value (1550−1600 kg/m$^3$) in this data is further compared to a typical biological anhydrous density of ≅1350 kg/m$^3$, from the experimentally feasible range of solution densities.

We can compare only the values reported for SC in Figure 6 and Table 1 to prior reports because literature data is not available for TDOC and DOC. First, checking consistency, the peak value of the sedimentation coefficient for our length and chirality sorted (6,5) rich sample is substantially greater than the peak valued measured by Arnold *et al.* for (6,5) SWCNTs.[27] This is expected, as the friction coefficient depends on the length of the nanotubes (longer SWCNTs move faster), and their reported average length is ≅ 1/4 the length of our sample. Our sample displays a peak sedimentation coefficient approximately equal to the peak value reported by Backes *et al.*;[29] however, this is not unexpected. Their sample contained contributions from larger diameter chiralities, which generally sediment faster, as well as bundles and other material. However, the value of the anhydrous density we measure for the (6,5) SWCNT in the SC dispersion is significantly lower than the value reported by either Backes *et al.* or Arnold *et al.*. There are at least two potential reasons for this discrepancy. The most likely is a different level of defects on the nanotube samples, which can affect the nanotube density, or potentially precision difficulties for the previous reports from broader distributions. We also note that neither of the literature references report explicit determination of the density and viscosity of their surfactant solutions, which in our measurements are measurably different from pure $D_2O$ values.

Comparison of the observed sedimentation coefficients and anhydrous densities of the SWCNT−surfactant complex in SC, DOC and TDOC provides further insight about the structural differences between the three surfactants. Because the nanotube population is identical in all samples, specific differences must be due to the quantity of adsorbed surfactant, and the adsorbed layer structure. A first observation is that although the anhydrous densities of the SWCNTs in DOC and SC are similar, the sedimentation coefficients themselves are significantly different, especially in 100% $H_2O$. Using eq 1, and remembering that length and thus the *L* part of $f/f_0$ are equivalent, $\rho_p$ is approximately the same, and $\eta$ and $\rho_s$ are explicitly accounted for, the increased sedimentation coefficient for SC is probably primarily due to a significantly thinner bound surfactant shell (smaller hydrodynamic radius) in SC than for the (6,5) SWCNT in DOC. Another possible

explanation is that the persistence length of the SWCNT is shorter in SC than in DOC.[35] A shorter persistence length would enable the SWCNTs to explore a distribution of conformations with reduced hydrodynamic drag and thus sediment faster. By similar logic, in TDOC the SWCNTs must also have a thinner hydrodynamic radius (or exhibit more flexibility) than in DOC, as well as have a greater quantity of adsorbed surfactant on the SWCNT than in SC. This is perhaps counterintuitive; however, to exhibit a less dense anhydrous partial specific density with a thinner radius than in SC, the addition of more TDOC molecules to the nanotube surface is required (the SWCNT component of the density is an identical property of the nanotube structure).[48]

Using our measured anhydrous density, and repeating the calculation of the surface packing density reported in Arnold *et al.*,[27] the estimated linear surface coverage is 4.46 ± 0.54, 4.64 ± 0.76, and 4.76 ± 0.83 molecules/nm for DOC, SC, and TDOC, respectively. Comparing to the value in Arnold *et al.*,[27] the surface coverage by SC on our SWCNT sample is estimated at 93 ± 15% (*versus* 72 ± 16%) of the SWCNT surface. The value used for the anhydrous density of the all the surfactants for these calculations was 0.745 mL/g.[49] Instead of relying on a literature value, we can extract $\bar{v}$ for each surfactant from measurable quantities (*vide infra*).

*Hydrated Buoyant Density Determination.* Separate from the anhydrous density, accurate measurement of the hydrated buoyant density in solutions containing density modifying agents is of interest for rational design of DGU separations in addition to other areas outside the scope of this contribution. Typically, the buoyant density of a SWCNT has been determined through observation of the nanotube species position at the end of a DGU experiment, noting that this buoyant density is for the effective particle as defined by the exclusion of the cosolute iodixanol from the hydrated surfactant layer on the nanotube. After extracting the correct fraction, the density of the bulk fraction is either measured directly (and assumed to be equal to the density of the hydrated surfactant–nanotube complex), or through the use of the refractive index or the absorbance change from the density medium. However, this methodology has several potential downfalls, including: the difficulty in pinpointing the isopycnic density due to the extinction of the driving force for sedimentation as the buoyancy difference goes to zero; the fact that the observed SWCNTs are typically in a macroscopically thick band, and diffusion, size differences, enantiomer distribution, or defects can all affect the observed location; the presence of a temporal and spatial gradient of viscosity that may additionally affect whether a position actually approximates equilibrium. An approach that circumvents these difficulties is to measure the sedimentation velocity in dilute solutions of the density modifier and extrapolate to the buoyant density.

**TABLE 1. Measured Anhydrous and Buoyant Densities of SWCNT Sample in Different Bile Salt Solutions[a]**

| | anhydrous density ($1/\bar{v}$, kg/m$^3$) | apparent anhydrous diameter (nm) ($\bar{v}_i$ = 0.745 cm$^3$/g) | buoyant density ($\rho$, kg/m$^3$) |
|---|---|---|---|
| 10 g/L DOC | 1574 ± 20 | 2.02 ± 0.09 | 1067.6 ± 2.3 |
| 10 g/L TDOC | 1527 ± 25 | 2.26 ± 0.15 | 1071.6 ± 2.3 |
| 10 g/L SC | 1561 ± 26 | 2.08 ± 0.12 | 1096.5 ± 4.7 |
| 10 g/L SC29 | 1786 | - | - |
| 20 g/L SC27 | 1890 ± 110 | 1.8 ± 0.15 | 1075 ± 25 |

[a] Anhydrous density, apparent anhydrous radius, and buoyant densities for the SWCNT sample as measured in 10 g/L surfactant; uncertainty is 1$\sigma$. Values from references were reported as $\bar{v}$ (units of cm$^3$/g), to aid comparison they have been converted to density values ($\rho = 1/\bar{v}$).

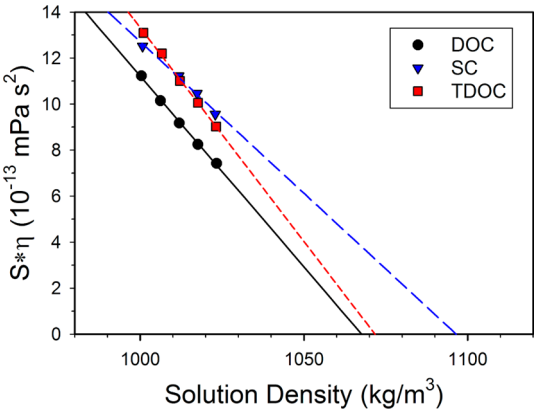


**Figure 7. Viscosity-corrected mean sedimentation coefficients for the (6,5) SWCNTs *versus* the density of the medium as adjusted by the amount of iodixanol present at a constant surfactant concentration of 10 g/L and for $H_2O$ as the solvent. For each of the three surfactants, DOC (black points, solid line), SC (blue triangles, long dashes), and TDOC (red squares, short dashes), the data is well fit by a straight line, indicating the surfactant structure is not being altered by the addition of iodixanol at the explored concentrations. From the slope of the change in $S \cdot \eta$ with the iodixanol content, the buoyant density of the SWCNT–surfactant complex can be extracted; the buoyant density is the value at which the fit line to the $S \cdot \eta$ data crosses the horizontal axis ($S = 0$).**

Distinct from the anhydrous density measurement, the hydrated buoyant density (in a specific medium) can be measured by adding a nonsolvating density modifying agent such as iodixanol. In this experiment, the effective density monitored for the SWCNT will include the volumetric contribution due to the water in the volume near the SWCNT from which the modifying agent is excluded.[30] Although more complicated systems can likely be devised, it is likely that for iodixanol this volume is effectively identical to the volume of the hydration shell of strongly correlated water surrounding/incorporated in the SWCNT–surfactant complex. Making this assumption, the effective average density within the volume including the hydration shell implies a substantially reduced

effective buoyant density (as compared to the anhydrous density measured by water isotope variation) for bile salt surfactant–SWCNT complexes in iodixanol solutions.

The experimental sedimentation coefficients and the linear best fit lines to the data for the SWCNT–surfactant complexes in iodixanol–surfactant solution are shown in Figure 7 with the extrapolated buoyant densities given in Table 1. In Figure 7, it is clear that the effective density difference driving sedimentation is dramatically reduced by use of iodixanol to modify the medium density rather than $D_2O$. Additionally, the data points are again well fit by the slope of the linear fit lines, indicating that, at least for dilute iodixanol concentrations, the iodixanol is not significantly affecting the hydrated surfactant structure. Greater iodixanol concentrations were not explored due to a lack of sample, experimental difficulties, and the more detailed data analysis necessary for co-sedimenting materials. For reference, iodixanol sediments with a $S \cong 0.5$ Sv (in the dilute limit, $H_2O$, 20 °C). To avoid the need to analyze the data with the co-sedimenting model, conditions that would result in the average SWCNT sedimentation coefficient being $\leq 6$ were avoided; for future work, negative sedimentation coefficients can also be measured and should be experimentally accessible at moderate iodixanol concentrations. As an experimental note, the sedimentation coefficients for the SWCNTs were determined using only $\cong 60\%$ of the radial absorbance range, avoiding the inner and outer regions in which concentration gradients first develop, such that the measured absorbance profiles reflected sedimentation through a uniform environment. The trends of the data and fit lines in Figure 7 are similar to the trends in the anhydrous density measurement, except that the DOC dispersion has the lowest buoyant density, followed by the TDOC and SC.

Comparing values for the buoyant density from our measurements to the literature, the buoyant density for the (6,5) nanotube in SC is in reasonable agreement with literature reports: Arnold *et al.*[27] reported for 20 g/L SC/iodixanol solution a buoyant density of 1075 ± 24 kg/m$^3$; Nair *et al.*[50] reported a best fit value of 1063.6 kg/m$^3$, also for 20 g/L SC; Ghosh *et al.*[7] reported a value $\cong$ 1068 kg/m$^3$ for 7 g/L SC; Wenseleers *et al.*[21] reported a value for $D_2O$, 7 g/L SC, Nycodenz solution of 1190 ± 5 kg/m$^3$, which we estimate as $\cong$ 1085 kg/m$^3$ in an equivalent $H_2O$ solution based on subtracting our measured density difference between $H_2O$ and $D_2O$ solutions. For DOC dispersed (6,5) SWCNTs: Wenseleers *et al.*[21] reported a value for $D_2O$, 7 g/L DOC, Nycodenz solution of 1210 ± 10 kg/m$^3$, which we estimate to be equivalent to $\cong$1105 kg/m$^3$ in an equivalent $H_2O$ solution; Zhao *et al.*[51] reported a value for a $H_2O$–$D_2O$ mixture, 5 g/L DOC, iodixanol solution of approximately 1110 kg/m$^3$. No literature values for the buoyant density of SWCNTs in TDOC/iodixanol solutions were found for comparison.

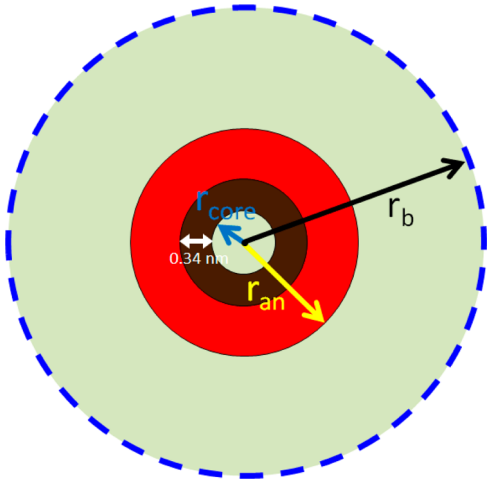


**Figure 8. Schematic explanation of the surfactant shell information. The nanotube–surfactant complex has multiple radial length scales. The anhydrous radius, $r_{an}$, effective hydrated radius, $r_b$, and the radius of the core, $r_{core}$, are depicted. The effective hydrodynamic radius is expected to be similar to the value of $r_b$.**

Comparing to the DOC literature results, it is surprising to us that the buoyant density values in both literature reports are greater than the buoyant density value in an equivalent SC solution. This is counter to our experience and current measurements. Possibilities for this variance between the values, beyond artifacts due to the DGU based measurement approach, include: the possibility that the iodixanol concentration affects the hydration shell at the higher concentrations used for isopycnic point based separation; differences in the density of the attached surfactant as a function of surfactant concentration or the level of SWCNT enantiomer enrichment; the effects of density modifier choice (iodixanol *versus* nycodenz); and possible variation of other contaminant cholate species concentration from different grades or suppliers of the raw surfactant.

Using a cylindrical mass balance model,[27] the difference in density between the buoyant and anhydrous densities can be used to measure the size of the hydration shell for each of the surfactant types. The simple mass balance, schematic in Figure 8, is

$$\rho_{buoyant} = \frac{\rho_{anhydrous}V_{anhydrous} + \rho_{hydration}V_{hydration} + \rho_{core}V_{core}}{V_{anhydrous} + V_{hydration} + V_{core}}$$
$$= \frac{\rho_{anhydrous}(r_{an}^2 - r_{core}^2) + \rho_{hydration}(r_b^2 - r_{an}^2) + \rho_{core}r_{core}^2}{r_b^2} \quad (5)$$

in which $r_{an}$ is the radius corresponding to the outer radius of the nanotube plus the bound surfactant shell,[52] $r_b$ is the outer radius of the hydration shell that determines the buoyant density, and $r_{core}$ is the radius of the internal cavity of the nanotube. The thickness of the SWCNT itself is taken to be 0.34 nm, and the diameter of the (6,5) SWCNT, carbon centers definition,

is 0.75 nm; $r_{core}$ is thus 0.205 nm. Given this information, eq 5 can be rearranged to be

$$r_b^2 = \frac{r_{an}^2(\rho_{hydration} - \rho_{anhydrous}) + r_{core}^2(\rho_{anhydrous} - \rho_{core})}{(\rho_{hydration} - \rho_{buoyant})} \quad (6)$$

Assuming that the density of the additional hydration and core volumes are equal to the average density of the surfactant solution in $H_2O$ (*i.e.*, $\rho_{hydration}$, $\rho_{core} \cong$ 1000 kg/m$^3$), the calculated values for the hydrated diameter from the measured anhydrous and buoyant densities using eq 6 are 5.79 ± 0.34, 6.09 ± 0.56, and 4.93 ± 0.36 nm for DOC, TDOC, and SC, respectively. These values are also tabulated in Table 2.

Interestingly, the calculated values for the apparent hydration radius do not fully follow the trend expected from the raw sedimentation rate of the nanotubes, ($r_{b,SC} < r_{b,TDOC} < r_{b,DOC}$), corresponding to the observed behavior ($S_{SC}$, $S_{TDOC} > S_{DOC}$). There are two probable causes for this discrepancy. One is that the effective hydrodynamic radius is not closely correlated to $r_b$, which is possible if the iodixanol is excluded/intercalated differently for the three surfactants; the second is that the literature value used for $\bar{v}$ of the surfactants (0.745 mL/g) from measurements for DOC and SC solutions is not uniformly applicable across the three surfactants (at least as adsorbed on the nanotube surface), particularly to TDOC for which we did not find a literature solution value. However, when we used a densitometer and methods from the literature to measure the $\bar{v}$ of our TDOC, we found it to be ≈0.75 mL/g.[53,54]

As an alternative to calculating $r_b$ from a $r_{an}$ calculated with $\bar{v}_i$, we can use eq 1 and assume that $r_b = r_{hydro}$ and use this to calculate $\bar{v}_i$. To use eq 1, however, we need to choose a model for the rotationally averaged friction coefficient of a rigid rod. Equation 7 is an approximation of the friction coefficient with length that better reflects the true dependence than the Broersma relation.[35]

$$\frac{a}{r_{hydro}} = \xi\left[\ln\left(\frac{4\xi}{e}\right)\right]^{-1} \times \left[\frac{1 - 0.782\psi + 0.691\psi^{1.67} + 0.622\psi^{1.77} + 0.418\psi^{2.16}}{1 - 0.677\psi + 1.601\psi^{2.07} + 0.178\psi^{2.26}}\right] \quad (7)$$

In eq 7, $\xi \equiv L/2r_{hydro}$ and $\Psi \equiv 1/\ln(\xi)$. If we combine eqs 1 and 7, we get[55]

$$S = \frac{\pi(r_{an}^2 - r_{core}^2)L \times (\rho_{anhydrous} - \rho_{hydration}) \times r_{hydro}}{6\pi\eta\xi\left[\ln\left(\frac{4\xi}{e}\right)\right]^{-1} \times \left[\frac{1 - 0.782\psi + 0.691\psi^{1.67} + 0.622\psi^{1.77} + 0.418\psi^{2.16}}{1 - 0.677\psi + 1.601\psi^{2.07} + 0.178\psi^{2.26}}\right]} \quad (8)$$

which can be rearranged to a monotonic function of $r_{hydro}$ and known values.

$$G(r_{hydro}) = \frac{\xi\left[\ln\left(\frac{4\xi}{e}\right)\right]^{-1} \times \left[\frac{1 - 0.782\psi + 0.691\psi^{1.67} + 0.622\psi^{1.77} + 0.418\psi^{2.16}}{1 - 0.677\psi + 1.601\psi^{2.07} + 0.178\psi^{2.26}}\right]}{r_{hydro}}$$

$$= \frac{(r_{an}^2 - r_{core}^2) \times L \times (\rho_{anhydrous} - \rho_{hydration})}{6\eta S} \quad (9)$$

Finding the values that satisfy eq 9 for the three surfactants yields $r_{hydro}$ equal to 2.47, 1.34, and 2.24 nm for DOC, SC, and TDOC, respectively. Setting $r_b = r_{hydro}$, $\bar{v}_i$ can then be calculated from the mass balance. Reasonable values for $\bar{v}_i$ are calculated in particular for DOC and TDOC (0.741, 1.133, and 0.794 L/kg for DOC, SC, and TDOC). Both sets of calculated values are also reported in Table 2. These values for the hydrodynamic radii do follow the order expected from the observed sedimentation velocities, although the value for SC in particular seems small, which propagates into a low anhydrous density value. A potential explanation for the remaining discrepancy is an exhibition of different persistence lengths in the three surfactants, which would enable the nanotubes to explore bent conformations that would increase their velocity relative to that expected for the same volume rigid rod. This implies that shorter SWCNTs should be explored as perhaps better candidates, particularly with the higher length resolution now available for shorter populations,[56] for rigorous AUC measurements.

*Effects of Surfactant Structure.* Although the structural parameters of the bound surfactant layers are the purpose of this contribution, the effects of the surfactant driven differences on the nanotube properties are also of interest. Literature studies have primarily used two methodologies to probe the quality of the surfactant packing, narrowness and intensity of the absorbance and fluorescence spectra, and reactivity in the presence of oxidizing agents. However, previous samples did not have independent measurements of the quantity of bound surfactant, which leads to ambiguity over the source of

**TABLE 2. Calculated Parameters from SWCNT Measureands[a]**

| | apparent fully hydrated diameter, $\bar{v}$ = 0.745 mL/g | apparent hydrodynamic diameter from *S* | apparent $\bar{v}$ from $r_{hydro}$ |
|---|---|---|---|
| 10 g/L DOC | 5.80 ± 0.30 nm | 4.94 nm | 0.741 L/kg |
| 10 g/L TDOC | 6.04 ± 0.46 nm | 4.53 nm | 0.794 L/kg |
| 10 g/L SC | 4.93 ± 0.35 nm | 3.10 nm | 1.133 L/kg |
| 20 g/L SC[27] | - | 5.5 ± 0.28 nm | 0.627 L/kg |

[a] Apparent fully hydrated diameter, $r_h$, from the mass balance with a literature $\bar{v}$ and the apparent $\bar{v}$ alternately calculated from the mode sedimentation coefficient; reported uncertainty is 1$\sigma$.

measured effects. Therefore we measured the absorbance and the NIR fluorescence of the SWCNT sample in the three surfactants to probe the effects of the surfactant shell on the optical properties. As described earlier, and shown in Supporting Information Figure S2, the absorbance spectra of the SWCNT sample in the three surfactant solutions was approximately unaffected by the choice of surfactant. The fluorescence intensities, shown in Figure 9, however, were affected by the nature of the dispersant. Compared to essentially identical emission intensities measured for resonant excitation of the (6,5) $E_{22}$ optical transition in DOC and TDOC, a 20% decrease in fluorescence intensity was observed for in SC.

Interestingly, a 20% lower intensity in fluorescence for SC dispersed SWCNTs is substantially less than the intensity difference measured for directly dispersed SWCNTs in SC instead of DOC (≅50%),[1] or for shorter, length sorted only, SWCNTs exchanged from DNA dispersion into DOC or SC (≅40% lower in SC, unpublished), but is similar to the value reported from single tube measurements on the (7,5) nanotube (≅25% lower in SC).[57] This may indicate a greater susceptibility to disruption of the surfactant packing of SC in the presence of nanotube defects. The fluorescence intensity and emission wavelength are expected to be strongly affected by the degree of surface isolation from the environment,[58−62] implying that the SC dispersed SWCNTs are worse at excluding quenchers than DOC or TDOC. This result is also consistent with literature reports utilizing reactants to probe the accessibility of the surfactant covered SWCNT surface. Hilmer *et al.*[63] monitored the accessibility of the surface *via* the reduction in bulk absorbance and fluorescence upon addition of a diazonium moiety to dispersed SWCNTs in solution including the (6,5). DOC and TDOC dispersed SWCNTs were found to be highly resistant to functionalization, while SC was found to be susceptible at significantly lower reactant concentrations. Siitonen *et al.*[57] also reported the use of aryl diazonium salt reactions to probe surfactant coverage effects at the single nanotube level on SC and DOC dispersed small diameter SWCNTs, primarily of the (7,5) species, using a NIR fluorescence microscope. In their results, DOC coated SWCNTs were found to exhibit greater fluorescence

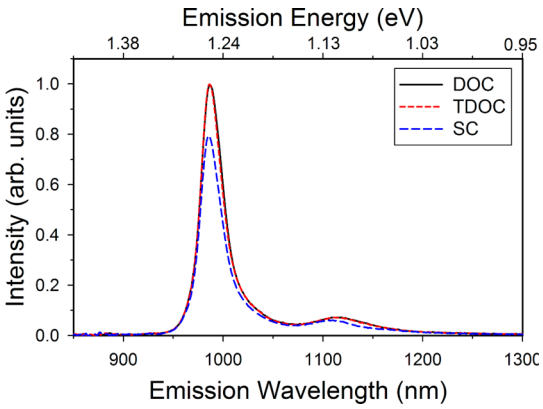


**Figure 9. Comparison of the NIR fluorescence intensity of the (6,5) SWCNT dispersed in each of the three different bile salts, as normalized by the peak intensity observed in DOC, at equal dilutions and excitation at 570 nm. DOC and TDOC dispersed (6,5) SWCNTs display indistinguishable fluorescence intensity, while the SC dispersed sample displays approximately 80% of the intensity. The peak emission wavelength is also slightly blue-shifted in SC dispersion, indicating a different dielectric environment near the SWCNT surface.**

intensity than SC dispersed SWCNTs. Additionally, they determined that the effective mean quenching range of an individual induced defect was greater in DOC than in SC; this indicated a longer exciton diffusion range and a more isolated nanotube surface with DOC dispersion that is also consistent with our observation.

The combined evaluation of the AUC determined information, along with the spectroscopic results, demonstrate the value of the information derivable from AUC. Both DOC and TDOC are demonstrated to better isolate the SWCNT surface than SC from the environment, but the AUC data informs us that this similar isolation is driven by different structures of the bound surfactant in the two cases. In DOC we infer that the stronger surface isolation, as compared to SC, is due to a more extended hydrated radius and bound surfactant structure; in TDOC the implication is that the surfactant coverage is denser on the SWCNT surface than in SC. This degree of information on bound structure, especially for chemically similar molecules, enables rational design of separations by identifying the actual structure that drives the observed phenomenon, as well as yielding comparative data for the development of bile salt appropriate force fields in molecular simulations.

## CONCLUSIONS

Analytical ultracentrifugation is demonstrated to enable extraction of both the anhydrous and buoyant densities of (6,5) single-wall carbon nanotubes in different, but closely related, bile salt surfactants and in the presence of the density modifying agent iodixanol. The values of the sedimentation coefficients extracted from the sedimentation in different density mixtures of $H_2O$ and $D_2O$ indicate that the structure of the bound surfactant layer does not change with deuteration of the

solvent, and that iodixanol similarly does not significantly incorporate into the surfactant shell, at least over the explored range of iodixanol concentrations.

Furthermore, the values for the anhydrous and buoyant densities extracted for the various bile salts indicate that the structures of the bound surfactant layers are significantly different for the three bile salt variants. The sedimentation data indicate that at 10 g/L surfactant concentration the DOC dispersed SWCNTs have the thickest bound layer of surfactant, with TDOC and SC each having thinner layers. TDOC, however, exhibited behavior indicating that it adsorbs at a higher surface density onto the nanotube surface than SC. This is apparent in the lesser anhydrous density of the SWCNT−TDOC complex, and logical correspondence to results from fluorescence measurements and previous surface reactivity studies. Additional value from this work is derived from its applicability to simulation studies and as an underlying data set for rational design of nanotube separations in an ultracentrifuge. Future work will extend the measurements described here as a basis for length distribution measurement, and to explore issues related to the mechanism of separation in co-surfactant DGU separations.

## METHODS[42]

Single-wall carbon nanotube powder was purchased from Southwest Nanotechnologies (SG65 grade, lot# SG65-000-0024). Sodium deoxycholate (99%, ACROS), sodium taurodeoxycholate (BioXtra grade >97%), sodium cholate hydrate (>99%), sodium dodecyl sulfate (SDS) and iodixanol ((5,5′-[(2-hydroxy-1-3-propanediyl)-bis(acetylamino)]-bis-[*N*,*N*′-bis(2,3dihydroxylpropyl-2,4,6-triiodo-1,3-benzenecarboxamide], sold as Opti-Prep) were acquired from Sigma-Aldrich and used without further purification. $D_2O$ (D > 99.8%) and $D_2{}^{18}O$ (D ≥ 98%, $^{18}O$ ≥ 97%) were purchased from Cambridge Isotopes.

SWCNTs were dispersed *via* tip sonication (1/4 in., 1 h, 0.9 W/mL) in an ice bath at a nominal concentration of 1.0 mg SWCNT/mL in 2.0% sodium deoxycholate solution. Following sonication, the resulting suspension was centrifuged in a high-speed centrifuge (Beckman J-2 centrifuge, JA-20 rotor, 1884 rad/s, 2 h) and the supernatant collected. This dispersion was then concentrated using pressurized stirred cells (Millipore) with ultrafiltration membranes (30 kDa MW cutoff), and then separated by length as reported previously.[64] Briefly, iodixanol was added to modify the bulk density, and the resulting dispersion was injected underneath a 10× larger volume layer of 1% DOC, 15% iodixanol solution layer in a centrifuge tube. For the SWCNTs described here, ≅20 separate length separations were conducted at 2650 rad/s (25.3 krpm) and 4 °C for 21 h in an Optima 80XL ultracentrifuge (Beckman-Coulter) with a swinging bucket rotor (Beckman SW-32Ti) and the maximal acceleration and deceleration profiles set to 4. Fractions were recovered by hand pipetting sequential layers and collecting like fractions. The samples in this work were extracted from the combinations of fractions 7 and 8 (of 20), *i.e.*, from a layer nearer the top of the liquid column and containing longer length (and/or more buoyant SWCNTs). This volume was several centimeters above the majority of the SWCNT mass in the separation. The SWCNTs reported on in Fagan *et al.*[64] were from fraction 13 and below. The pressurized stirred cells were used to concentrate the separated population and to remove most of the iodixanol.

Chirality separation was performed using a modified version of the methods reported by Ghosh *et al.*[7] and Blackburn *et al.*[65] Briefly, SC solution was added to the concentrated length fractionated dispersion to bring the surfactant concentration to 5 g/L DOC and 10 g/L SC. This liquid (≅0.9 mL) was then layered on top of a race layer of 12.63% iodixanol, 0.71% SC and 0.177% SDS (4 mL) in optiseal centrifuge tubes (Beckman #362185) and centrifuged in a VTi 65.2 vertical rotor. Separation was conducted at 6806 rad/s (65 krpm) for 1.5 h at 20 °C using the maximum acceleration profile and deceleration profile 1. During centrifugation, the SWCNTs sediment through the race layer at a rate dependent on their chirality, enantiomeric handedness, length, defect density and morphology; the SWCNTs used in this work were collected from the pink-purple band including the slowest sedimenting nanotubes in the separation. Photographs of the separation are provided in the SOL. Like fractions were combined from 15 separations and exchanged using multiple concentration/dilution steps in the ultrafiltration cell into 10 g/L DOC, 18 MΩ $H_2O$. At this stage the amount of iodixanol was removed below detectable levels (<0.1 μg/mL), and the final SWCNT concentration was brought to approximately 35 μg/mL (est. extinction coefficient of 2.06 A/(mm mg/mL) at 775 nm). Exchange of the DOC for TDOC or SC surfactants was also performed utilizing the stirred ultrafiltration cell. In both cases, approximately 400 μL of the SWCNT−DOC sample was added to 2.5 mL of either 10 g/L TDOC or SC solution, stirred, and then the liquid in the cell was completely expressed (hold up volume is ≅100 μL according to the manufacturer) to remove the initial DOC content. The SWCNTs were then immediately redispersed through agitation (using a pipettor) with added 10 g/L TDOC or SC surfactant (4 mL), stirred, and then concentrated in steps with stirring/agitation breaks to approximately 450 μL. From a volumetric basis, the DOC content after exchange was estimated as <0.05 g/L. These samples were additionally further diluted by a minimum of 3:1 with additional TDOC or SC solution prior to AUC measurement. Therefore, final samples were estimated to have a surfactant composition of approximately 99.9% TDOC or SC. Note, however, that this is a greater % dilution than the claimed purity of the bulk surfactant from the manufacturer, and thus, the actual composition of the surfactant is more accurately described as asymptoted to the composition of the surfactant powder.

UV−vis-NIR absorbance spectra were collected on a Cary 5000 UV−vis-NIR spectrometer from 1880 to 185 nm in 1 nm increments through a 1 mm quartz cuvette with an integration time of 0.1 s/nm (2 nm slit width). The spectra of the corresponding blank surfactant solution samples were collected separately and linearly subtracted during data analysis.

NIR fluorescence was measured on a Horiba Jobin-Yvon nanolog-3 spectrofluorometer with a liquid nitrogen cooled InGaAs array detector and a 450 W xenon lamp. Excitation was selected using a dual grating monochromotor with 1200 (grooves/mm) × 500 (blaze, nm) gratings, and a slit selected bandpass of 5 nm. Emission was measured in the right angle geometry with a 5 mm × 5 mm square quartz cuvette through a long-pass filter and dispersed with a 100 × 800 grating onto the array detector. Bandpass for the emission side was set to 5 nm. Integration time was 60 s (slice) or 12 s (contour plot). Collected spectra were corrected for the wavelength dependent irradiance of the excitation beam, and the wavelength dependence of the long pass filter and detector train as calibrated to a NIST traceable lamp. For the surfactant comparison in Figure 9, an appropriate amount of the sample was diluted with additional surfactant solution to yield a dilute sample with an absorbance of 0.01/cm (0.02/cm for the contour plot) at 775 nm in 10 g/L of the appropriate surfactant and 20% (by volume) $D_2O$. Under these conditions, in-filter effects affecting the monitored emission intensity should be minimal.

The spontaneous Raman backscattered light was collected in a collinear 180° backscattering configuration on the sample dispersed in DOC with a triple grating spectrometer (Dilor XY800) and a liquid nitrogen cooled CCD detector. An Ar+ laser (Coherent Innova Sabre with multiline visible head) provided the 514.5 nm excitation, and was also used in multiline mode to

excite a dye laser (Coherent) for the excitation at 570.7 nm; in each case, approximately 10 mW of power was focused to a spot size of approximately 100 $\mu$m within the liquid sample volume. Benzonitrile was used as a reference standard to ensure wavenumber accuracy. Raman frequency shifts in the range from approximately 100 to 3500 $cm^{-1}$ were measured, covering the region of spectral shift in which radial breathing modes (RBM), D band, G band, G′ (2D) and water Raman features occur. The integration time was 10 s, and at each grating position was collected 3×. The D/G ratio was calculated using the peak values of the $G^+$ and D features after subtraction of a linear and sloped background respectively. The backgrounds were taken as the nonresonant signal averaged from 2040 to 2077 $cm^{-1}$, covering 100 data points, for the G band, and as sloped line between the measured signal averaged over the region 1172−1194 $cm^{-1}$ and the average over the region from 1402 to 1420 $cm^{-1}$.

Analytical ultracentrifugation was performed on a Beckman-Coulter XLI analytical ultracentrifuge in an AN-50 8 cell rotor with 2-sector Epon-charcoal centerpieces. The optical path length of these cells is 1.2 cm. Data was collected in sedimentation velocity mode with both the interference optics and absorption optics at centrifugation speeds between 733 rad/s (7000 rpm) and 4188 rad/s (40 000 rpm) at 20 °C; most data was collected at 2617 rad/s (25 krpm) or 2932 rad/s (28 krpm). After preliminary experiments to confirm the absence of SWCNT concentration effects at the desired dilution levels, SWCNT dispersions for AUC measurement were diluted with either $H_2O$-surfactant, $D_2O$-surfactant, and/or $H_2O$-iodixanol-surfactant solutions to reach the desired concentration using a pipettor at a single fixed volume. Dilution was typically 4:1 (surfactant solution/SWCNT dispersion) to reach an appropriate concentration yielding an absorbance of ≅0.8 A at the desired wavelength across the AUC cell. Either water or the surfactant solution was used as the reference depending on the experiment. No differences in the extracted sedimentation coefficient distribution measured were observed based on the wavelength chosen for the absorbance monitoring (235, 305, 347, or 570 nm). Most measurements were conducted at 305 ± 2 nm (uncertainty reflects the instrument's specification), except in the case for solutions containing iodixanol, which were measured at 570 ± 2 nm. The wavelength was not varied during any experiment, however, so within an experiment the wavelength was a constant. Generally a radial scan for each cell was recorded every 5 min. Typical data sets covering the entire sedimentation process included between 85 scans and 105 scans, depending on the density difference and the viscosity of the medium. Viscosities and densities of the various surfactant and surfactant-iodixanol solutions were measured independently with an Anton Parr 5000 M densitometer/Lovis ME viscometer combination instrument or a combination of an Anton Parr 5000 M densitometer and an AMVn viscometer instrument at 20 °C. In some cases, viscosities and densities for intermediate compositions were linearly interpolated between measured $H_2O$-surfactant and $D_2O$-surfactant values. Density and viscosity values were directly measured for each parent solution diluted to form the final solutions of the various combinations of isotopes, surfactants, and iodixanol. These are reported in Table S1 of the SOL.

Sedimentation data was analyzed with the software packages SEDFIT version 14.0c. This version of SEDFIT corrects for an instrumental time-stamping error that was recently uncovered.[66] The c(S) model or c(S, ff0) were used to extract the distribution of $S$ values represented in the measured data. Similar distributions were extracted with either model. $S$ values were fitted over the range of 0−20 Sv (200 divisions), using the measured or extrapolated solution viscosity and density values and an $f/f_0$ value of 8.725 (DOC), 8.9 (SC) and 8.45 (TDOC) as these were the best fit values found for the SWCNTs in $H_2O$ (averaging output values reported for initial guess values above and below these best fit values). In tests, the supplied $f/f_0$ value did not significantly affect the reported $S$ distribution. Regularization was fixed at $P = 0.683$. The position of the meniscus was generally well-defined, and changed only minimally when allowed to float during fit optimization. For anhydrous density measurements, the fitting window was maximized to include as much of the sedimentation volume as possible. For buoyant density measurements, the fitting was limited to approximately the middle 60% of the sedimentation volume, biased closer to the meniscus, to ignore regions with significantly changing iodixanol concentrations. After initial optimization of the c(S) analysis in SEDFIT using an estimated $\bar{v}$, the analysis was performed using the experimentally determined $\bar{v}$ value; these values are shown in the figures, no significant change to the $\bar{v}$ value was found from the iteration.

*Conflict of Interest:* The authors declare no competing financial interest.

*Acknowledgment.* C. Khripin thanks support of a National Research Council Postdoctoral fellowship.

*Supporting Information Available:* Additional optical characterization of the SWCNT sample, AFM images and histograms, and a table of the used viscosity and density values are reported. This material is available free of charge *via* the Internet at http://pubs.acs.org.

## REFERENCES AND NOTES


1. Haggenmueller, R.; Rahatekar, S. S.; Fagan, J. A.; Chun, J.; Becker, M. L.; Naik, R. R.; Krauss, T.; Carlson, L.; Kadla, J. F.; Trulove, P. C.; et al. Comparison of the Quality of Aqueous Dispersions of Single Wall Carbon Nanotubes using Surfactants and Biomolecules. *Langmuir* **2008**, *24*, 5070.
2. Wenseleers, W.; Vlasov, I. I.; Goovaerts, E.; Obraztsova, E.; Lobach, A. S.; Bouwen, A. Efficient Isolation and Solubilization of Pristine Single-Walled Nanotubes in Bile Salt Micelles. *Adv. Funct. Mater.* **2004**, *14*, 1105–1112.
3. Zheng, M.; Jagota, A.; Semke, E. D.; Diner, B. A.; McLean, R. S.; Lustig, S. R.; Richardson, R. E.; Tassi, N. G. DNA-Assisted Dispersion and Separation of Carbon Nanotubes. *Nat. Mater.* **2003**, *2*, 338.
4. Tu, X.; Manohar, A.; Jagota, A.; Zheng, M. DNA Sequence Motifs for Structure Specific Recognition and Separation of Carbon Nanotubes. *Nature* **2009**, *460*, 250–253.
5. Arnold, M. S.; Stupp, S. I.; Hersam, M. C. Enrichment of Single-Walled Carbon Nanotubes by Diameter in Density Gradients. *Nano Lett.* **2005**, *5*, 713.
6. Arnold, M. S.; Green, A. A.; Hulvat, J. F.; Stupp, S. I.; Hersam, M. C. Sorting Carbon Nanotubes by Electronic Structure using Density Differentiation. *Nat. Nanotechnol.* **2006**, *1*, 60–65.
7. Ghosh, S.; Bachilo, S. M.; Weisman, R. B. Advanced Sorting of Single-Walled Carbon Nanotubes by Nonlinear Density-Gradient Ultracentrifugation. *Nat. Nanotechnol.* **2010**, *5*, 443–450.
8. Yanagi, K.; Miyata, Y.; Kataura, H. Optical and Conductive Characteristics of Metallic Single-Wall Carbon Nanotubes with Three Basic Colors; Cyan, Magenta, and Yellow. *Appl. Phys. Express* **2008**, *1*, 034003.
9. Nish, A.; Hwang, J.; Doig, J.; Nicholas, R. J. Highly Selective Dispersion of Single-Walled Carbon Nanotubes using Aromatic Polymers. *Nat. Nanotechnol.* **2007**, *2*, 640–646.
10. Fagan, J. A.; Becker, M. L.; Chun, J.; Hobbie, E. K. Length Fractionation of Carbon Nanotubes using Centrifugation. *Adv. Mater.* **2008**, *20*, 1609.
11. Fagan, J. A.; Becker, M. L.; Chun, J.; Nie, P.; Bauer, B. J.; Simpson, J. R.; Walker, A.R. H.; Hobbie, E. K. Centrifugal Length Separation of Carbon Nanotubes. *Langmuir* **2008**, *24*, 13880.
12. Sun, X. M.; Zaric, S.; Daranciang, D.; Welsher, K.; Lu, Y. R.; Li, X. L.; Dai, H. J. Optical Properties of Ultrashort Semiconducting Single-Walled Carbon Nanotube Capsules Down to Sub-10 nm. *J. Am. Chem. Soc.* **2008**, *130*, 6551–6555.
13. Khripin, C. Y.; Arnold-Medabalimi, N.; Zheng, M. Molecular-Crowding-Induced Clustering of DNA-Wrapped Carbon Nanotubes for Facile Length Fractionation. *ACS Nano* **2011**, *5*, 8258–8266.
14. Fagan, J. A.; Bauer, B. J.; Hobbie, E. K.; Becker, M. L.; Hight Walker, A. R.; Simpson, J. R.; Chun, J.; Obrzut, J.; Bajpai, V.; Phelan, F. R.; et al. Carbon Nanotubes: Measuring Dispersion and Length. *Adv. Mater.* **2011**, *23*, 338–348.

15. Liu, J.; Hersam, M. C. Recent Developments in Carbon Nanotube Sorting and Selective Growth. *MRS Bull.* **2010**, *35*, 315.
16. Niyogi, S.; Densmore, C. G.; Doorn, S. K. Electrolyte Tuning of Surfactant Interfacial Behavior for Enhanced Density-Based Separations of Single-Walled Carbon Nanotubes. *J. Am. Chem. Soc.* **2009**, *131*, 1144–1153.
17. Hároz, E. H.; Rice, W. D.; Lu, B. Y.; Ghosh, S.; Hauge, R. H.; Weisman, R. B.; Doorn, S. K.; Kono, J. Enrichment of Armchair Carbon Nanotubes *via* Density Gradient Ultracentrifugation: Raman Spectroscopy Evidence. *ACS Nano* **2010**, *4*, 1955–1962.
18. O'Connell, M. J.; Bachilo, S. M.; Huffman, C. B.; Moore, V. M.; Strano, M. S.; Haroz, E. H.; Rialon, K. L.; Boul, P. J.; Noon, W. H.; Kittrell, C.; et al. Band-Gap Fluorescence from Individual Single-Walled Carbon Nanotubes. *Science* **2002**, *297*, 593–596.
19. Moore, V. C.; Strano, M. S.; Haroz, E. H.; Hauge, R. H.; Smalley, R. E.; Schmidt, J.; Talmon, Y. Individually Suspended Single-Walled Carbon Nanotubes in Various Surfactants. *Nano Lett.* **2003**, *3*, 1379–1382.
20. Green, A. A.; Duch, M. C.; Hersam, M. C. Isolation of Single-Walled Carbon Nanotube Enantiomers by Density Differentiation. *Nano Res.* **2009**, *2*, 69.
21. Cambré, S.; Wenseleers, W. Separation and Diameter-Sorting of Empty (End-Capped) and Water-Filled (Open) Carbon Nanotubes by Density Gradient Ultracentrifugation. *Angew. Chem., Int. Ed.* **2011**, *50*, 2764–2768.
22. Fagan, J. A.; Huh, J. Y.; Simpson, J. R.; Blackburn, J. L.; Holt, J. M.; Larsen, B. A.; Walker, A. R. H. Separation of Empty and Water-Filled Single-Wall Carbon Nanotubes. *ACS Nano* **2011**, *5*, 3943–3953.
23. Crochet, J.; Clemens, M.; Hertel, T. Optical Properties of Structurally Sorted Single-Wall Carbon Nanotube Ensembles. *Phys. Status Solidi B* **2007**, *244*, 3964–3968.
24. Quintillá, A.; Hennrich, F.; Lebedkin, S.; Kappes, M. M.; Wenzel, W. Influence of Endohedral Water on Diameter Sorting of Single-Walled Carbon Nanotubes by Density Gradient Centrifugation. *Phys. Chem. Chem. Phys.* **2010**, *12*, 902–908.
25. Carvalho, E. J. F.; dos Santos, M. C. Role of Surfactants in Carbon Nanotubes Density Gradient Separation. *ACS Nano* **2010**, *4*, 765–770.
26. Bonaccorso, F.; Hasan, T.; Tan, P. H.; Sciascia, C.; Privitera, G.; Di Marco, G.; Gucciardi, P. G.; Ferrari, A. C. Density Gradient Ultracentrifugation of Nanotubes: Interplay of Bundling and Surfactants Encapsulation. *J. Phys. Chem. C* **2010**, *114*, 17267–17285.
27. Arnold, M. S.; Suntivich, J.; Stupp, S. I.; Hersam, M. C. Hydrodynamic Characterization of Surfactant Encapsulated Carbon Nanotubes Using an Analytical Ultracentrifuge. *ACS Nano* **2008**, *2*, 2291–2300.
28. Mächtle, W.; Börger, L. *Analytical Ultracentrifugation of Polymers and Nanoparticles*; Springer Laboratory: New York, NY, 2006.
29. Backes, C.; Karabudak, E.; Schmidt, C. D.; Hauke, F.; Hirsch, A.; Wohlleben, W. Determination of Surfactant Density on SWCNTs by Analytical Ultracentrifugation. *Chem.—Eur. J.* **2010**, *16*, 13176–13185.
30. Brown, P. H.; Balbo, A.; Zhao, H.; Ebel, C.; Shuck, P. Density Contrast Sedimentation Velocity for the Determination of Protein Partial-Specific Volumes. *PLoS One* **2011**, *6*, e26221.
31. The potential for H−D exchange, well described in ref 30, is discussed in Methods section.
32. Weisman, R. B.; Bachilo, S. M. Dependence of Optical Transition Energies on Structure for Single-Walled Carbon Nanotubes in Aqueous Suspension: An Empirical Kataura Plot. *Nano Lett.* **2003**, *3*, 1235–1238.
33. Cambré, S.; Schoeters, B.; Luyckx, S.; Goovaerts, E.; Wenseleers, W. Experimental Observation of Single-File Water Filling of Thin Single-Wall Carbon Nanotubes Down to Chiral Index (5,3). *Phys. Rev. Lett.* **2010**, *104*, 207401.
34. Maultzsch, J.; Telg, H.; Reich, S.; Thomsen, C. Radial Breathing Mode of Single-Walled Carbon Nanotubes: Optical Transition Energies and Chiral-Index Assignment. *Phys. Rev. B* **2005**, *72*, 205438.
35. Mansfield, M. L.; Douglas, J. F. Transport Properties of Rodlike Particles. *Macromolecules* **2008**, *41*, 5422–5432.
36. Carney, R. P.; Kim, J. Y.; Qian, H.; Jin, R.; Mehenni, H.; Stellacci, F.; Bakr, O. M. Determination of Nanoparticle Size Distribution Together with Density or Molecular Weight by 2D Analytical Ultracentrifugation. *Nat. Commun.* **2011**, *1338*, 1–8.
37. Lees, E. E.; Gunzburg, M. J.; Nguyen, T. L.; Howlett, G. J.; Rothaker, J.; Nice, E.; Clayton, A. H. A.; Mulvaney, P. Experimental Determination of Quantum Dot Size Distributions, Ligand Packing Densities, and Bioconjugation Using Analytical Ultracentrifugation. *Nano Lett.* **2008**, *8*, 2883–2890.
38. Jamison, J. A.; Krueger, K. M.; Mayo, J. T.; Yavuz, C. T.; Redden, J. J.; Colvin, V. L. Applying Analytical Ultracentrifugation to Nanocrystal Suspensions. *Nanotechnology* **2009**, *20*, 1–10.
39. Sousa, A. A.; Morgan, J. T.; Brown, P. H.; Adams, A.; Jayasekara, M. P. S.; Zhang, G.; Ackerson, C. J.; Kruhlak, M. J.; Leapman, R. D. Synthesis, Characterization, and Direct Intracellular Imaging of Ultrasmall and Uniform Glutathione-Coated Gold Nanoparticles. *Small* **2012**, *8*, 2277–2286.
40. Falabella, J. B.; Cho, T. J.; Ripple, D. C.; Hackley, V. A.; Tarlov, M. Characterization of Gold Nanoparticles Modified with Single-Stranded DNA Using Analytical Ultracentrifugation and Dynamic Light Scattering. *Langmuir* **2010**, *26*, 12740–12747.
41. Zook, J. M.; Rastogi, V.; MacCuspie, R. I.; Keene, A. M.; Fagan, J. Measuring Agglomerate Size Distribution and Dependence of Localized Surface Plasmon Resonance Absorbance on Gold Nanoparticle Agglomerate Size Using Analytical Ultracentrifugation. *ACS Nano* **2011**, *5*, 8070–8079.
42. Certain equipment, instruments or materials are identified in this paper in order to adequately specify the experimental details. Such identification does not imply recommendation by the National Institute of Standards and Technology nor does it imply the materials are necessarily the best available for the purpose.
43. Schuck, P. Size Distribution Analysis of Macromolecules by Sedimentation Velocity Ultracentrifugation and Lamm Equation Modeling. *Biophys. J.* **2000**, *78*, 1606–1619.
44. Brown, P. H.; Schuck, P. Macromolecular Size-and-Shape Distributions by Sedimentation Velocity Analytical Ultracentrifugation. *Biophys. J.* **2006**, *90*, 4651–4661.
45. See www.analyticalultracentrifugation.com.
46. Crochet, J.; Clemens, M.; Hertel, T. Quantum Yield Heterogeneities of Aqueous Single-Wall Carbon Nanotube Suspensions. *J. Am. Chem. Soc.* **2007**, *129*, 8058.
47. Hartleb, H.; Kröker, K.; Hertel, T. Density Gradient Ultracentrifugation and Stability of SWNT−Peptide Conjugates. *Chem. Phys. Lett.* **2012**, *535*, 131–135.
48. A similar thought experiment is attaching a few helium balloons to a bowling ball, attaching each balloon adds to the total mass of the combined object, but also reduces the volume averaged density.
49. Fontell, K. Micellar Behaviour in Solutions of Bile-Acid Salts. *Kolloid Z. Z. Polym.* **1971**, *246*, 614–625.
50. Nair, N.; Kim, W.; Braatz, R. D.; Strano, M. S. Dynamics of Surfactant-Suspended Single-Walled Carbon Nanotubes in a Centrifugal Field. *Langmuir* **2008**, *24*, 1790–1795.
51. Zhao, P.; Einarsson, E.; Lagoudas, G.; Shiomi, J.; Chiashi, S.; Maruyama, S. Tunable Separation of Single-Walled Carbon Nanotubes by Dual-Surfactant Density Gradient Ultracentrifugation. *Nano Res.* **2011**, *4*, 623–634.
52. This is more properly described as the outer radius of the annular volume necessary to contain the measured volume of surfactant attached to the nanotube in the anhydrous density measurement. Note that the surfactant is not required to be all within this radius of the nanotube.
53. Kratky, O.; Leopold, H.; Stabinger, H. The Determination of the Partial Specific Volume of Proteins by the Mechanical Oscillator Technique. *Methods Enzymol.* **1973**, *27*, 98–110.

54. Lee, J. C.; Timasheff, S. N. Partial Specific Volumes and Interactions with Solvent Components of Proteins in Guanidine Hydrochloride. *Biochemistry* **1974**, *13*, 257–265.
55. Note that the anhydrous sedimentation coefficient and buoyant sedimentation coefficient are identical at the 10 g/L surfactant−100% $H_2O$ composition; either density can be used for velocity calculations at this point as long as the volume used is self-consistent.
56. Khripin, C. Y.; Tu, X.; Heddleston, J. M.; Silvera-Batista, C.; Hight Walker, A. R.; Fagan, J.; Zheng, M. High-Resolution Length Fractionation of Surfactant-Dispersed Carbon Nanotubes. *Anal. Chem.* **2013**, *85*, 1382–1388.
57. Siitonen, A. J.; Tsyboulski, D. A.; Bachilo, S. M.; Weisman, R. B. Surfactant-Dependent Exciton Mobility in Single-Walled Carbon Nanotubes Studied by Single-Molecule Reactions. *Nano Lett.* **2010**, *10*, 1595–1599.
58. Ju, S.; Kopcha, W. P.; Papadimitrakopoulos, F. Brightly Fluorescent Single-Walled Carbon Nanotubes *via* an Oxygen-Excluding Surfactant Organization. *Science* **2009**, *323*, 1319.
59. Choi, J. H.; Strano, M. S. Solvatochromism in single-walled carbon nanotubes. *Appl. Phys. Lett.* **2007**, *90*, 223114.
60. Silvera-Batista, C. A.; Wang, R. K.; Weinberg, P.; Ziegler, K. J. Solvatochromic Shifts of Single-Walled Carbon Nanotubes in Nonpolar Microenvironments. *Phys. Chem. Chem. Phys.* **2010**, *12*, 6990–6998.
61. Larsen, B. A.; Deria, P.; Holt, J. M.; Stanton, I. N.; Heben, M. J.; Therien, M. J.; Blackburn, J. L. Effect of Solvent Polarity and Electrophilicity on Quantum Yields and Solvatochromic Shifts of Single-Walled Carbon Nanotube Photoluminescence. *J. Am. Chem. Soc.* **2012**, *134*, 12485–12491.
62. Aguirre, C. M.; Levesque, P. L.; Paillet, M.; Lapointe, F.; St-Antoine, B. C.; Desjardins, P.; Martel, R. The Role of the Oxygen/Water Redox Couple in Suppressing Electron Conduction in Field-Effect Transistors. *Adv. Mater.* **2009**, *21*, 3087.
63. Hilmer, A. J.; McNicholas, T. P.; Lin, S. C.; Zhang, J. Q.; Wang, Q. H.; Mendenhall, J. D.; Song, C. S.; Heller, D. A.; Barone, P. W.; Blankschtein, D.; et al. Role of Adsorbed Surfactant in the Reaction of Aryl Diazonium Salts with Single-Walled Carbon Nanotubes. *Langmuir* **2012**, *28*, 1309–1321.
64. Fagan, J. A.; Lin, N. J.; Zeisler, R.; Hight Walker, A. R. Effects of Gamma Irradiation for Sterilization on Aqueous Dispersions of Length Sorted Carbon Nanotubes. *Nano Res.* **2011**, *4*, 393–404.
65. Blackburn, J. L.; Holt, J. M.; Irurzun, V. M.; Resasco, D. E.; Rumbles, G. Confirmation of K-Momentum Dark Exciton Vibronic Sidebands Using $^{13}$C-labeled, Highly Enriched (6,5) Single-walled Carbon Nanotubes. *Nano Lett.* **2012**, *12*, 1398–1403.
66. Zhao, H.; Ghirlando, R.; Piszczek, G.; Curth, U.; Brautigam, C. A.; Shuck, P. Recorded Scan Times Can Limit the Accuracy of Sedimentation Coefficients in Analytical Ultracentrifugation. *Anal. Biochem.* [Online early access]. DOI: 10.1016/j.ab.2013.02.011. Published online: Feb 28, 2013.